Journal of Research in Medical and Dental Science
2022, Volume 10, Issue 9, Page No: 96-103

Available Online at: www.jrmds.in
eISSN No. 2347-2367: pISSN No. 2347-2545

Using of Image Registration Software Packages in Segmentation of left Ventricle Tissues in SPECT Images

Yousif M Abdallah*

Department of Radiological science and Medical Imaging, College of Applied Medical Science, Majmaah University, Al-Majmaah, Saudi Arabia

ABSTRACT

Background: Medical imaging has been widely used as a key method for the diagnosis, evaluation, and monitoring of the treatment of myocardial pathologies. Nuclear medicine imaging plays an important role in the morphological and physiological assessment of cardiac tissues. The performance of the left ventricular muscles was evaluated using the gated studies series (rest and stress tests).

Methods: In this study, a semi- and fully automated registration approach were used to segment cardiac tissues and quantify the left ventricle dysfunction.

Results: The image registration of medical image studies will be combined with a computational method to robotically compute a set of features from the myocardial SPECT images. These features will be used in statistical studies and cataloguing of scanned people to healthy and unhealthy patients.

Conclusion: Image registration, segmentation, and characterization approaches were used in this study. The results of all computation processes were assessed and deliberated.

Key words: Nuclear medicine, Segmentation, Left ventricle, SPECT, Image

HOW TO CITE THIS ARTICLE: Yousif M Abdallah, Using of Image Registration Software Packages in Segmentation of left Ventricle Tissues in Spect Images, J Res Med Dent Sci, 2022, 10 (9):96-103.

Corresponding author: Yousif M Abdallah

e-mail✉**:** y.yousif@mu.edu.sa

Received: 01-September-2022, Manuscript No. JRMDS-22-73376;

Editor assigned: 03-September-2022, **PreQC No.** JRMDS-22-73376(PQ);

Reviewed: 19-September-2022, QC No. JRMDS-22-73376(Q);

Revised: 22-September-2022, Manuscript No. JRMDS-22-73376(R);

Published: 29-September-2022

INTRODUCTION

Nuclear medicine physicians must have a firm grip on visual interpretation to recognize and diagnose anomalies, as well as a firm grasp on border and criterion evaluation [1-2]. Likewise, myocardial infusion SPECT image interpretation includes an atlas, but it covers the theoretical foundations in greater detail. Individuals with major blood circulation disorders have a more distinct endocardial shape, but endocardial edge identification is erroneous [3-4]. Individuals with smaller hearts may have imprecise measurements, whereas those with larger hearts may have more precise measurements. These studies used a combination of computer simulations and experiments [5]. Additionally, the left ventricular volume is segmented with distinct cardiac zones inside each segment, as is the left ventricle ejection fraction (LVEF) of the heart. New techniques are being used to determine left ventricular diastolic indices and mass [6-7]. The patient's left ventricle (LV) perfusion pattern was observed using novel polar mapping technology, and areas of hypoperfusion were identified using a second method. It is a technique for visualizing the maximum three-dimensional (3D) LV count distribution on a two-dimensional polar map. It is critical to observe that the polar intensity at the base of the LV is on the periphery of the polar map, whereas the polar intensity at the apex of the LV is within its heart [8-10]. The tracer accumulation ratio of the patient's cardiac 3D model was compared to a lower statistically established normal limit for ventricle's volume or function, which is less than the tracer accumulation ratio of the patient's cardiac 3D model [11-12]. Calculating the degree of hypoperfusion is feasible using a blackout or a polar map. The hypoperfused segments were identified and counted [13-14]. Due to the varied forms of the LV, coronary artery mapping using computed tomography may be more accurate than standard computed tomography in determining LV perfusion [15]. Depending on the study, most heart perfusion studies report data in segments of 17 or 20 segments. The basal, middle and apical thirds of the cardiac perfusion zone were split into three segments according to the 20-segment model: the basal,

middle, and apical thirds, with the apical cap divided into two segments. While 30% of the foundation is built at the base, 30% of the foundation is composed of the intermediate capillary zone, and 40% of the foundation is composed of the apex and apical cap [16-17]. There is a correlation between coronary artery blood flow and segmental distribution of the coronary arteries of the heart. The left anterior descending artery is divided into the following sections: one, second, third, seventh, eighth, and thirteenth; the right artery is divided into the following sections: four, nine, ten, six, and seventeen; and the right coronary artery is divided into the following sections: seventeen, twelve, six, six, and twelve [18-20]. Individual variables, such as data collection, data processing, quantification, and physiological variation, affect the reproducibility of results. For example, complex data must be used to run these programs for easy analysis. To analyze and scrutinize the data, a subject matter expert (SME) with a strong professional background in statistics and visualization is required [21-23]. Radiotracers are frequently used to map the physiology and fluid streams of a tissue or organ because they aid in the diagnosis of physiological conditions in the body. Compared to techniques such as computed tomography and nuclear imaging, which can produce images of structures that are not present, emission tomography modes simultaneously examine perfusion and metabolic activity [24-25]. Anesthesiologists, cardiologists, and psychiatrists use SPECT to diagnose and confirm certain medical conditions. In addition to improving image acquisition and analysis methods, critical areas of research include increasing the spatial and temporal resolution of digital medical images, which can be accomplished using higher resolutions. However, it should be noted that effective image analysis is not possible until new or more integrated registration methods are developed [27-30]. Combining images acquired from multiple viewpoints, time acquisitions, and even subject atlases with a variety of medical imaging modalities, such as positron emission tomography (PET), single-photon computed tomography (SPECT), computed tomography, and magnetic resonance imaging (MRI), enables the detection of anatomical differences (MRI). When used in conjunction with other techniques, SPECT can be used to assess both myocardial perfusion and ventricular function. Because image processing and quantification aided in the development of the diagnostic and prognostic capabilities of myocardial perfusion imaging, Among the additional imaging techniques are the enhancement of perfusion data, enhancement of overall information, assessment of feasibility, and sequential follow-up following therapy [31-33].

METHODS

The study population consisted of patients (18–68 years) who were admitted to the nuclear medicine department of Elnieleen Medical Center, Khartoum, Sudan. All data were collected for nuclear examinations performed after patient preparation, and all procedures were performed before scanning. A solution that automatically computes and uses a series of features from SPECT myocardial perfusion images to conduct statistical analyses and classify images as belonging to or not belonging to subjects with myocardial infusion has been developed as a result of the integration of image recording and other computational techniques for medical image analysis. The researcher will review the image registration algorithms that were used in detail, including the transformation, similarity measure, optimization, and interpolator algorithms, in addition to the segmentation and segmentation steps. When image classification methods are used in conjunction with the feature subset of the segmentation method, the diagnostic performance of the system significantly improves. The steps involved in developing a computational solution can be divided into the following categories. The alignment of the slices under investigation in the gated myocardial perfusion SPECT images with the pre-built template image is called data registration. Statistical analysis and image classification are called image classification. Subsequently, each step and the experimental results obtained at each stage are thoroughly explained. With this implementation, it is not intended to replace physicians' clinical judgment but rather to assist them in clinical decision-making, for example, by supplementing cardiology medicine teaching. SPECT image is developed for the visualization of the heart for photos that must be identified to have a consistent collection of images. While developing something, it is possible to follow three distinct phases. Images of patients in good health, ill, and very ill are shown. Individuals who did not feel well were photographed. Each of the three steps begins with a segmented coronary artery map and each of the three steps ends with another segmented coronary artery map. The template image contained 12 slices that were used for each cardiac axis in this study. Four-dimensional template myocardial perfusion SPECT images were created from myocardial SPECT imaging data collected from healthy volunteers who provided information regarding the location of their coronary arteries. The 3D template image was selected based on the data from the dataset. We then determined how the answers of the control group were compared with the control image. The output of the recording technique is used to construct the template image and only one template image was created in this instance. The architecture of the heart will differ depending on the sex of the patient. Fixed pictures should be described using a cubic B-spline interpolator, which allows the user to choose the origin, distance, direction, and size of the image by adjusting the interpolator parameters. A moving image must pass through to function effectively. An image intensity filter that rescales the images was used to equalize the intensity of the images. This was followed by the registration process. Specifically, the phrase "split into two pieces" refers to two distinct pre-registration methods: one that is rigid and employs a pre-registration approach, and the other that is deformable and employs the most effective pre-registration methodology for

multi-resolution registrations Figure1.

According to Bayes' theorem, execution of the algorithm results in the development of various geometric dimensions. Because mathematical models are employed to validate a medical practitioner's clinical diagnosis, they are sometimes referred to as clinical decision-support systems in specific circles, such as the medical community. All examinations were performed using SPECT machine on a notebook computer equipped with an Intel Core i5-5200U CPU (4.0GHz) and 8 GB of RAM, and this computation was carried out in Mat Lab (64-bit). Several image processing and classification technologies, including MatLab (2021b) and the Insight Toolkit (ITK) 4.3, was used to implement the image segmentation procedure.

RESULTS

This experimental study was conducted in Sudan to characterize myocardial diseases using an image-processing technique. The study was performed on 80 patient's myocardial images in order to help in the improvement of accurate heart tissue recognition, interpretation, and patient diagnosis and the data were analyzed using the MatLab program. Early computer technology included the use of computational image registration techniques to build a SPECT myocardial perfusion template for SPECT myocardial perfusion imaging. The doctor double-checked the SPECT model photograph to ensure that the registration procedure had been followed properly. The stress and relaxation segments are depicted in the SPECT images in Figures 2 using k-means clustering.

It was necessary to align the coronary artery mapping with the template slices to generate the picture slices for manual mapping. The results of the clinical stress protocol (as well as the results of the remaining assessments) are depicted in Figures 3 and 4.

The effectiveness of this method can be calculated. Initially, a 40-slice SPECT stress-myocardial image was segmented into 40 slices using the segmentation, and a gold standard was created. For the first time, an approach has been developed from scratch. This separation was made possible by the application of four

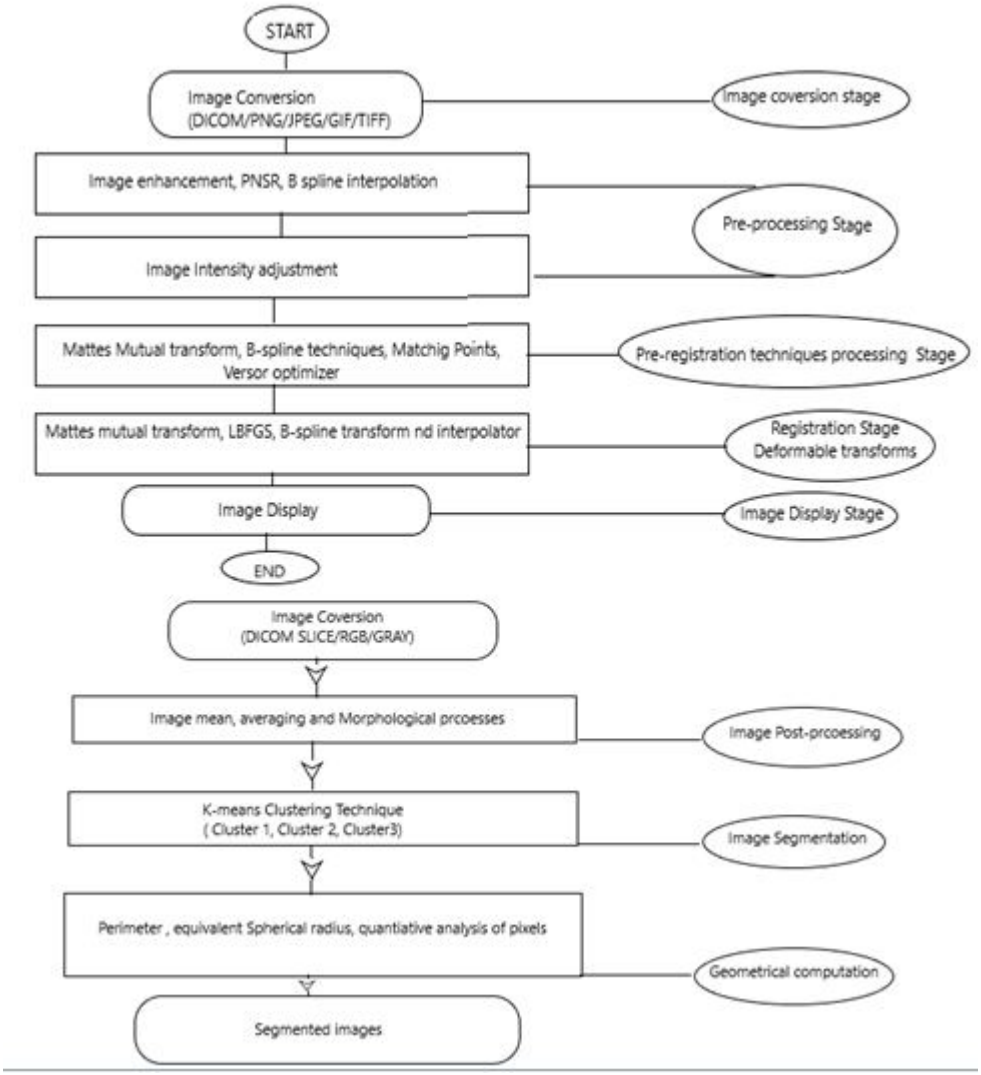

Figure 1: Segmentation and registration algorithms.

independent processes, two of which were automatic in nature. Each accessible threshold is composed of three levels and three K-mean clusters, and there are many thresholds at each of these levels Figure 5 and Figure 6. In the MATLAB simulation results listed in Table 1, the estimated Dice coefficient can be seen as a percentage of the simulation results. The same slices used in the first half of this example were also segmented and reviewed manually by a clinical practitioner in the second section. Table 2 summarizes the results of Dice's coefficient calculations.

The K-means approach can be utilized to determine the Dice coefficient. Following the application of K-means clustering (three clusters) to the myocardial SPECT

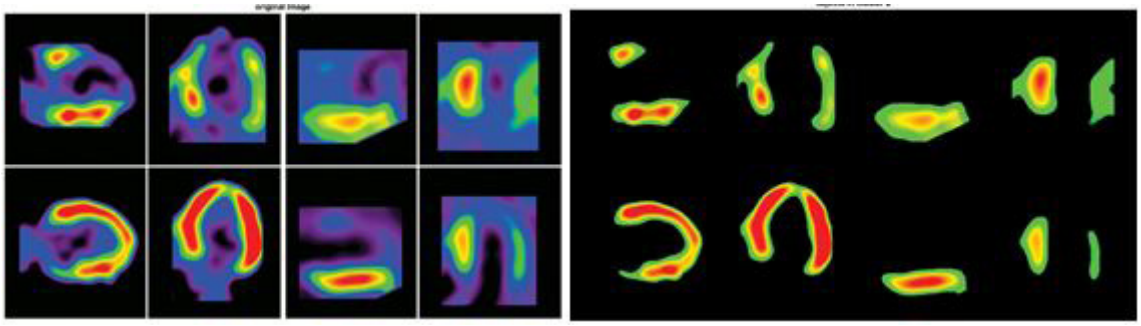

Figure 2: Segmented SPECT image obtained using k-means clustering techniques.

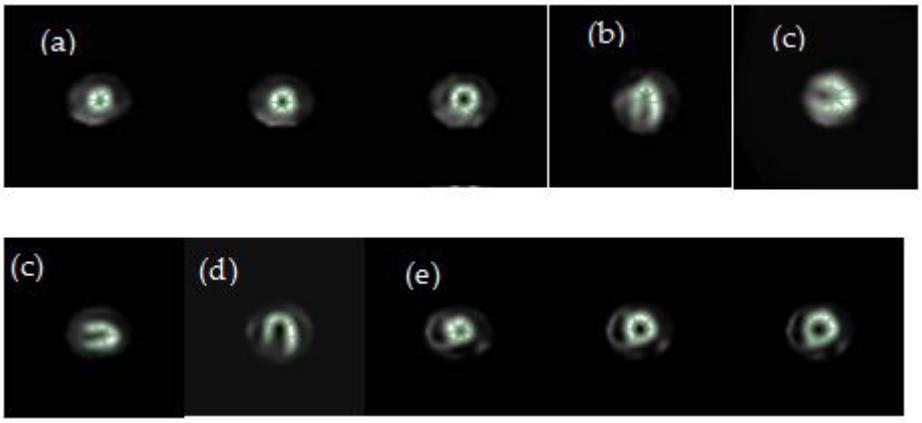

Figure 3: Segmented SPECT studies (stress studies): (a) SA; (b) HLA; (c) VLA and rest studies: (c) SA; (d) HLA; (e) VLA.

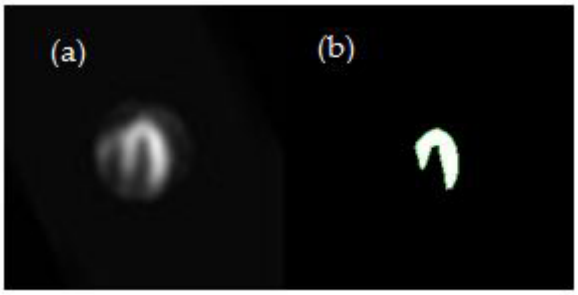

Figure 4: Cardiac segmented using thresholding technique (Otsu's technique).

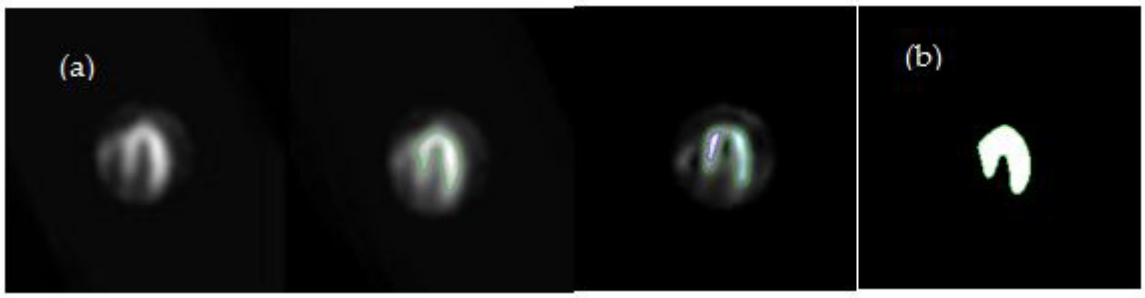

Figure 5: Water shedding segmentation technique: (a) Original image; (b) Segmented image.

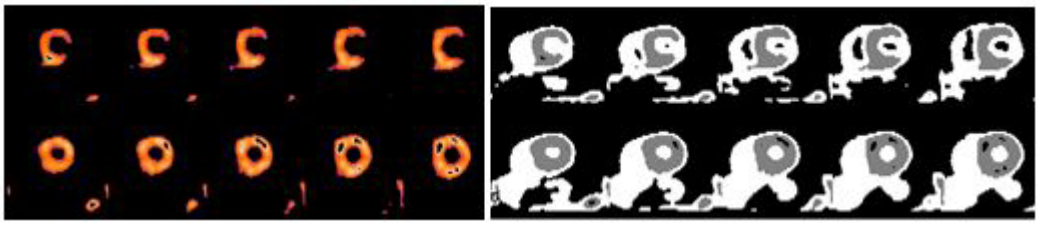

Figure 6: K-means segmentation process applied on color cardiac images.

Table 1: Comparison between the automatic, manual segmentation (ten physicians) and Dice's coefficient computation (N=80 patients).

Features	Manual Score	Automated scores using matlab program			
		Otsu' algorithm	K-means Assembling	Region Growing	Shape Detection
Mean	0.604	0.768	0.783	0.747	0.819
Std. Dev.	0.092	0.059	0.057	0.038	0.057

Table 2: Geometric measurements of the segmented images (N=80 patients).

Procedure	Axis	Perimeter	Equivalent Spherical Radius	Roundness	Elongation	Number of Pixels
Stress	SA	267.07 ± 55.7	29.23 ± 7.4	0.80 ± 0.04	1.14 ± 0.4	643.88 ± 74.8
	HLA	246.22 ± 45.4	28.11 ± 8.3	0.75 ± 0.08	1.43 ± 0.9	585.8 ± 78.1
	VLA	286.45 ± 60.1	34.09 ± 9.2	0.82 ± 0.05	1.26 + 0.7	902.27 ± 104.6
Rest	SA	283.04 ± 42.6	29.37 ± 8.8	0.82 ± 0.03	1.49 ± 0.7	629.86 ± 101.5
	HLA	309.81 ± 52.4	40.04 ± 7.9	0.79 ± 0.02	1.71 ± 0.9	806.52 ± 99.8
	VLA	296.26 ± 48.6	33.39 ± 6.8	0.84 ± 0.07	1.46 ± 0.8	982.7 ± 109.7

Table 3: Quantitative analysis of segmented images VLA geometric vs. and Bayesian tests results with for both stress and rest exam.

Parameter	Perimeter	Equivalent Spherical Radius	Roundness	Elongation	Number of Pixels	Algorithm Classification	Final Algorithm Classification	Clinical Analysis
				Stress scan				
Mean	564.71	62.42	0.82	1.31	2087.34	Normal	Normal	Normal
Std. Dev.	115.7	9.7	0.09	0.5	531.7	--	--	--
				Stress scan				
Mean	564.71	62.42	0.82	1.31	2087.34	Normal	Normal	Normal
Std. Dev.	92.69	15.07	0.09	0.08	502.06	--	--	--

Table 4: Bayesian classifier results and confusion matrix.

	Algorithm judgment	Abnormality present	Abnormality not present
Clinical decision	Abnormality present	29	13
	Abnormality not present	9	53

segment template, useful myocardial infusion geometric metrics such as perimeter, spherical equivalent, roundness, elongation, and pixel count can be determined, which can be used to improve the accuracy of myocardial infusion imaging. Table 3 shows the mean values for each geometric dimension per axis for the stress and resting images.

To evaluate the categorization technique, the terms "abnormality present" and "abnormality not present" are used interchangeably. According to the confusion matrix provided in table 6, the values for healthy and sick individuals. The sensitivity, specificity, accuracy, and mean error rate were tested in addition to the five criteria. The findings were placed through their pace. The parameters determined are listed in the preceding table, and the values obtained are listed in Table 4.

DISCUSSION

The aim of this experimental study was to characterize myocardial diseases in Sudan using image processing techniques. In addition, it helps improve accurate heart tissue recognition, interpretation, and patient diagnosis. Eighty patients who fulfilled certain criteria related to cardiac pathology were selected. Using serial SPECT images, the researcher created a template image and performed left ventricular segmentation of the core using the template image. This study aimed to determine whether a typical left ventricular infusion had a specific geometric dimension and, using statistical analysis, to determine whether patients had a cardiac issue. Participants were separated into two groups for discussion. Initially, rigid transforms are used to pre-register the model, which is followed by registration using deformable transforms and, ultimately, registration with rigid transforms. To correct global deformations before applying these sequential registration methods to localized deformations, they must first be applied to global deformations. Owing to significant anatomical differences between male and female patients, it was challenging to identify components that consistently provided reliable data in both groups. Even when used in

conjunction with other approaches, linear interpolators result in visually disturbing distortions when compared to the original data. Because of the curve fit and interactive curve design, the B-spline interpolator produced the best results while also being the most precise of the three interpolators. Although deformable registration methods are essentially based on data theory metrics, they are exceedingly flexible and adaptive to a broad variety of adjustments, and as such, they are employed in a huge number of stiff registration procedures. The algorithm deals with the mutual information between Mattes and his friends. Visual confirmation was performed on both the SPECT coronary artery map template and contemporaneous SPECT myocardial infusion template to ensure that they were correct. Because of the non-uniform image intensity, typical image processing techniques such as binary thresholding and gradient segmentation cannot be used for cardiac SPECT data. As indicated in Tables 1 to Table 4, clinical professionals produced the best results when they employed the Golden Standard and manual segmentation, as well as when they used K-means clustering methods with three clusters and the Dice coefficient. The approximate area increases in both size and scope. However, to improve the accuracy of population segmentation, these variables must be more closely related to the Dice coefficient than they currently are. These numbers were correct in all cases. As seen in this example, a basic and successful segmentation strategy begins with picture enhancement, which is accomplished using advanced morphological and morphometric algorithms that decrease noise and clarify borders. Other data, such as lung and breast activity tracer retention, were unaffected and were consistent with a normal, non-hypertrophied right ventricle in the LV segment, as in this case. According to the images in figures 2–6, the LV can be distinguished from the right ventricle in all the sections. The boundaries of the division components were delineated with great precision, applying geometric and statistical factors related to the categorization of the problem. Table 4 displays the mean stress and residual images for each geometric dimension, as well as the overall stress values and residual images for the entire geometric dimension. To obtain the remaining measurements, the middle template's coronary artery mapping portion is segmented into numerous slices that have already been registered, thereby increasing the geometrical dimensions of each template, which are measured from the base to the apical portion of the coronary artery. A single slice was used as a reference for all sections because of this alignment. This established a consistent link between the initial and final geometric dimensions of the patient evaluation and the segmented structure geometric dimensions used by related classes, thereby altering the classification outcomes. In accordance with Bayesian classification, the system has a reasonable capacity for detecting abnormalities, with a detection rate of approximately 70 percent. Without an abnormality, the false-positive ratio of the algorithm, or its ability to declare a healthy test, is approximately 95%. The mean and standard deviation of the classification approach was lower than the total number of healthy patients who completed the test using the test data package. As a result of the decreased sample size of the test data package that was employed, it is possible to justify the lower mean and standard differential values in the classification. The accuracy and precision features of the system revealed that the system can accurately determine myocardial diseases in 83% and 88% of the cases, respectively. All aspects of the procedure, particularly patient images and image template recording, which have been visually examined and are therefore more likely to be detected as having variability, should be tweaked to obtain an average error rate of 12.4%. When the situation becomes more serious, small hearts have appropriate myocardial perfusion, whereas large hearts have insufficient myocardial perfusion. These are the most frequently encountered causes of the average error rate. The geometrical dimensions of the LV may change as a result of this adjustment, leading to erroneous reporting that could result in unwanted distortions. The classification system that was put in place was successful. The term 'categorizing someone' refers to someone who categorizes other people. To overcome this issue, the photo registration technique described in this article has been refined and improved. In a clinical study, the average time required for each set of HLA, VLA, or SE photos for the calculation of patient and clinical protocol images was 8 minutes per set of photos (stress or rest). A possible explanation for this statistic is the restricted CPU power of the machine utilized to develop the computer solution. Because there is no known SPECT image pattern in the scientific literature, one must be generated from the scratch. Hence, it was decided to design a method based on deformable transformations to provide myocardial SPECT imaging both during stress and at rest. A study was conducted to determine the quantity and location of cardiac anomalies in patients' coronary arteries using myocardial SPECT perfusion imaging. The results were manually identified and reported. LV nuclear research segmentation is a time-consuming and labor-intensive procedure used to diagnose cardiac problems. It demands a great deal of patience and effort from the patient. The automatic estimation of the Dice coefficient is possible using the K-means clustering technique described below (three clusters). Despite the range of topologies revealed by the findings, it is recommended that the Dice coefficient be increased to near maximum values for all datasets comprising coronary artery mapping regions to obtain the best results. In comparison to other technologies, the constancy of the functioning of this technique is crucial, as it can endure interference from low-resolution and noisy data. Although men and women have a large variety of physical characteristics, the data suggest that the computational method may be capable of producing high-quality cardiac SPECT images for men and women with a wide variety of anatomical characteristics. It is feasible to address two key issues in

the field of SPECT image processing easily by utilizing a single mathematical solution: noise and low-level features, which are explored below. Owing to the high specificity and accuracy of the classifier, it is necessary to improve the image collection approaches to boost the sensitivity while minimizing the calculation time. This is critical for increasing the sensitivity and error rate of the classifier.

ACKNOWLEDGMENT

The authors are thankful to the Deanship of Scientific Research, at Majmaah University for funding this research.

CONFLICT OF INTEREST

No potential conflict of interest relevant to this article was reported. Funding: This work was supported by the Deanship of Scientific Research, at Majmaah University for funding this research.

REFERENCES

1. https://www.intechopen.com/books/advances-and-applications-in-deep-learning/advancements-in-deep-learning-theory-andapplicationsperspective-in-2020-and-beyond (2021). Accessed 18 July 2021
2. https://arxiv.org/abs/2010.05719
3. https://arxiv.org/abs/2005.11074
4. Ahmad M, Abdullah M, Moon H, et al. Image classification based on automatic neural architecture search using binary crow search algorithm. IEEE Access 2020; 8:189891-912.
5. Wang N, Gao Y, Chen H, et al. Nas-fcos: Fast neural architecture search for object detection. In proceedings of the IEEE/CVF conference on computer vision and pattern recognition 2020; 11943-11951.
6. Weng Y, Zhou T, Li Y, et al. Nas-unet: Neural architecture search for medical image segmentation. IEEE Access 2019; 7:44247-4457.
7. Wistuba M, Rawat A, Pedapati T. Automation of deep learning-Theory and practice. In Proceedings of the 2020 International Conference on Multimedia Retrieval 2020; 5-6.
8. Nahid AA, Mehrabi MA, Kong Y. Histopathological breast cancer image classification by deep neural network techniques guided by local clustering. Bio Med Res Int 2018; 2018.
9. Pal R, Saraswat M. Histopathological image classification using enhanced bag-of-feature with spiral biogeography-based optimization. Appl Intell 2019; 49:3406-3424.
10. Oyelade ON, Ezugwu AE, Venter HS, et al. Abnormality classification and localization using dual-branch whole-region-based CNN model with histopathological images. Comput Biol Med 2022; 105943.
11. Zhang Z, Si D, Zhang Q, et al. Prophylactic rivaroxaban therapy for left ventricular thrombus after anterior ST-Segment elevation myocardial infarction. JACC Cardiovasc Interv 2022; 15:861-872.
12. Xu S, Lu H, Cheng S, et al. Left ventricle segmentation in cardiac MR images via an improved ResUnet. Int J Biomed Imaging 2022; 2022:8669305.
13. Hu H, Pan N, Wang J, et al R. Automatic segmentation of left ventricle from cardiac MRI via deep learning and region constrained dynamic programming. Neurocomputing 2019; 347:139-148.
14. Khan A, Iskandar DN, Chai WY, et al. A new technique for reducing the segmentation error of left ventricle contours using magnetic resonance images. In2021 International Conference on Frontiers of Information Technology (FIT) 2021; 269-274.
15. Xu S, Cheng S, Min X, et al. Left ventricle segmentation based on a dilated dense convolutional networks. IEEE Access 2020; 8:214087-97.
16. Shaaf ZF, Jamil MM, Ambar R, et al. Automatic left ventricle segmentation from short-axis cardiac MRI images based on fully convolutional neural network. Diagnostics 2022; 12:414.
17. Aly AH, Khandelwal P, Aly AH, et al. Fully automated 3d segmentation and diffeomorphic medial modeling of the left ventricle mitral valve complex in ischemic mitral regurgitation. Med Image Anal 2022; 80:102513.
18. Abdelrauof D, Essam M, Elattar M. Light-weight localization and scale-independent multi-gate UNET segmentation of left and right ventricles in mri images. Cardiovasc Eng Technol 2022; 13:393-406.
19. Krishnaswamy D, Hareendranathan AR, Suwatanaviroj T, et al. A new semi-automated algorithm for volumetric segmentation of the left ventricle in temporal 3d echocardiography sequences. Cardiovasc Eng Technol 2022; 13:55-68.
20. Wisneski AD, Wang Y, Cutugno S, et al. Left ventricle biomechanics of low-flow, low-gradient aortic stenosis: A patient-specific computational model. Front Physiol 2022; 13:848011.
21. Liu H, Zhuang Y, Song E, et al. A bidirectional multilayer contrastive adaptation network with anatomical structure preservation for unpaired cross-modality medical image segmentation. Comput Biol Med 2022; 105964.
22. Militello C, Rundo L, Toia P, et al. A semi-automatic approach for epicardial adipose tissue segmentation and quantification on cardiac CT scans. Comput Biol Med 2019; 114:103424.
23. Bui V, Hsu LY, Shanbhag SM, et al. Improving multi-atlas cardiac structure segmentation of computed tomography angiography: A performance evaluation based on a heterogeneous dataset. Comput Biol Med 2020; 125:104019.
24. Pang S, Pang C, Zhao L, et al. SpineParseNet: Spine parsing for volumetric MR image by a two-stage segmentation framework with semantic image representation. IEEE Transactions on Medical Imaging.

2020 Sep 21;40(1):262-73.

25. Ma Z, Wu X, Wang X, et al. An iterative multi-path fully convolutional neural network for automatic cardiac segmentation in cine MR images. Med Phys 2019; 46:5652-5665.
26. Ammar A, Bouattane O, Youssfi M. Automatic cardiac cine MRI segmentation and heart disease classification. Comput Med Imaging Graph 2021; 88:101864.
27. Tan LK. Fully automated segmentation of the left ventricle in cine cardiac magnetic resonance imaging. Doctoral dissertation, University of Malaya.
28. Tan LK, McLaughlin RA, Lim E, et al. Fully automated segmentation of the left ventricle in cine cardiac MRI using neural network regression. J Magn Reson Imaging 2018; 48:140-152.
29. Sun X, Garg P, Plein S, et al. SAUN: Stack attention U-Net for left ventricle segmentation from cardiac cine magnetic resonance imaging. Med Phys 2021; 48:1750-1763.
30. Böttcher B, Beller E, Busse A, et al. Fully automated quantification of left ventricular volumes and function in cardiac MRI: Clinical evaluation of a deep learning-based algorithm. Int J Cardiovasc Imaging 2020; 36:2239-2247.
31. Aly AH, Khandelwal P, Aly AH, et al. Fully automated 3D segmentation and diffeomorphic medial modeling of the left ventricle mitral valve complex in ischemic mitral regurgitation. Med Image Anal 2022; 80:102513.
32. Moura-Ferreira S, Sampaio F, Ribeiro J, et al. A rare case series of mitral valve clefts diagnosed by 3D echocardiography and mini-review of the literature. Echocardiogr 2019; 36:1203-1207.
33. Luo G, An R, Wang K, et al. A deep learning network for right ventricle segmentation in short-axis MRI. In Computing in Cardiology Conference 2016; 485-488.